INVESTIGATION OF DYNAMIC NOISE AFFECTING GEODYNAMICS INFORMATION IN A TETHERED SUBSATELLITE

NASA GRANT NAG5-458

Final Report

For the period 1 August 1984 through 31 July 1985

Principal Investigator

Dr. Gordon E. Gullahorn

July 1985

Prepared for
National Aeronautics and Space Administration
Greenbelt, Maryland 20771

Smithsonian Institution
Astrophysical Observatory
Cambridge, Massachusetts 02138

The Smithsonian Astrophysical Observatory
is a member of the
Harvard-Smithsonian Center for Astrophysics

The NASA Technical Officer for this Grant is Mr. Jean E. Welker, Code 921 Earth Survey Applications Division, Goddard Space Flight Center, Greenbelt, Maryland 20771.

INVESTIGATION OF DYNAMIC NOISE AFFECTING GEODYNAMICS INFORMATION IN A TETHERED SUBSATELLITE

NASA GRANT NAG5-458

Final Report

For the period 1 August 1984 through 31 July 1985

Principal Investigator

Dr. Gordon E. Gullahorn

July 1985

Prepared for
National Aeronautics and Space Administration
Greenbelt, Maryland 20771

Smithsonian Institution
Astrophysical Observatory
Cambridge, Massachusetts 02138

The Smithsonian Astrophysical Observatory is a member of the Harvard-Smithsonian Center for Astrophysics.

The NASA Technical Officer for this Grant is Mr. Jean E. Welker, Code 921 Earth Survey Applications Division, Goddard Space Flight Center, Greenbelt, Maryland 20771.

CONTENTS

1.0 INTRODUCTION:

This Semiannual Status Report summarizes the work performed under Grant NAG5-458 entitled "Investigation of Dynamic Noise Affecting Geodynamics Instrumentation in a Tethered Subsatellite."

During the reporting period, SAO has

- Written an invited paper to be published in the forthcoming Special Issue on Geodynamics of the IEEE Transactions on Geoscience and Remote Sensing.
- Continued modeling of the atmospherically induced dynamic noise in the subsatellite through the modification and use of the SKYHOOK program; interaction with an elementary form of random atmosphere was simulated.
- Developed a method for stabilizing the subsatellite against the rotational effects of atmospheric perturbations and analyzed a simplified model.
- Performed a variety of analytic studies of tether dynamics aimed at elucidating dynamic noise processes and at continuing the rotational stabilization analysis.
- Discovered a novel mechanism for coupling longitudinal and latitudinal oscillations of the tether: a longitudinal (approximately vertical) oscillation causes an oscillation in the subsatellite's altitude; this, in turn, causes an oscillation in the drag experienced, which is in the horizontal (latitudinal) direction.
- Begun study of random vibration analysis for modeling the TSS under atmospheric perturbation.

2.0 INVITED REVIEW PAPER

A paper entitled "Gravity Gradiometry from the Tethered Satellite System", by G. E. Gullahorn, F. Fuligni and M. D. Grossi, was written and submitted for the Special Issue on Geodynamics of IEEE Transactions on Geoscience and Remote Sensing. This paper has been accepted and is scheduled for publication in the July, 1985 issue. It has been modified substantially from the draft version included as an appendix to the Semiannual Report.

Our survey of the open (published) literature showed virtually nothing on the topic of TSS gravity gradiometry; even among less readily available sources such as contract and grant reports or limited distribution summaries of meetings, nothing at an introductory level was found. Thus, in keeping with the spirit of a "Special Issue" intended for a broad audience, we decided to write a largely tutorial/review paper rather than simply report one or two current results comprehensible only to a few other specialists. We did, however, also summarize some SAO work in the field.

Although researching and writing this paper was a substantial effort, we believe that the product was valuable. It will publicize the concepts and advantages of TSS gradiometry (and of space-born gradiometry platforms in general), and provide a ready entrée for the fledgling researcher as well as the interested scientist from a related field.

2.1 The Significance Of Platform Rotation

The discipline of producing such a review was also of value to the authors. The process of TSS gradiometry, and the role of dynamic noise calculations, was placed in context. The important role of rotation of the instrument platform (subsatellite) was examined and emphasized. Excerpting some paragraphs from the paper:

The gravity gradient is a tensor whose components in Cartesian coordinates are defined as

$$\Gamma_{ij} = \partial g_i/\partial x_j = - \partial^2 U/\partial x_i \partial x_j \qquad (2.1.1)$$

The gravity gradient is expressed in Eötvös units, 1 E = 10^{-9} gal/cm = 10^{-9} sec^{-2}. Note that because the gravity vector arises from a potential, $\Gamma_{ij} = \Gamma_{ji}$; and in free space Poisson's equation will relate the three diagonal components, $\Gamma_{xx} + \Gamma_{yy} + \Gamma_{zz} = 0$. Thus, of the nine components, only five are truly independent.

Measurements made with an instrument linearly accelerated relative to a rest frame will not be affected due to the phenomenon of common mode rejection discussed below. However, if the instrument is subject to a rotation with angular velocity $\vec{\omega}(t)$, the measured gradient will be

$$\Gamma^{meas} = \Gamma^{rest} + \dot{T} + T^2 \qquad (2.1.2)$$

where Γ^{rest} is the gradient of (2.1.1), T(t) is the matrix

$$T(t) = \begin{bmatrix} 0 & -\omega_3 & \omega_2 \\ \omega_3 & 0 & -\omega_1 \\ -\omega_2 & \omega_1 & 0 \end{bmatrix} \qquad (2.1.3)$$

and T^2 means matrix multiplication in the common sense. Note that the term dependent on the angular <u>acceleration</u> is anti-symmetric and can be immediately distinguished from the inertial frame gradient if the full tensor gradient is measured accurately enough; the term dependent on the angular <u>velocity</u> is symmetric, and cannot be removed from the observations without knowledge of the instrument's rotation.

If the gradiometer is not attached to a completely motionless platform, the measured gradient may contain errors. A linear acceleration, with no rotation, is relatively innocuous due to the phenomenon of "common mode rejection": the two test masses will be subject to the same non-gravitational acceleration, so the difference, the measured gradient, will not be affected. Rotation of the instrument, however, will <u>innately</u> alter the sensed gradient as shown by (2.1.2). If the rotation has angular velocity $\omega(t)$, ignoring for simplicity the vector nature, then the T^2 term of (2.1.2) will have magnitude approximately ω^2. Measurements at the goal level of 3×10^{-4} E = 3×10^{-13} sec^{-2} will be degraded if $\omega \geq 5.5 \times 10^{-7}$ sec^{-1} = 0.1 deg/hr. Stability at this level should be readily achievable, and if not, such rotational velocities can be easily measured and their effect removed via (2.1.2). The rotational acceleration term, $\dot{T}$, however, will interfere with measurements if $\dot{\omega} \geq 3 \times 10^{-13}$ sec^{-2}; to subtract the effects would require, over a one second integration, knowledge of ω to about 3×10^{-13} sec^{-1} = 6×10^{-8} deg/hr, well beyond current technology. If eight of the nine components of Γ are measured, the rotational acceleration effects can be removed by their anti-symmetry. However, even a very small $\dot{\omega}$

will generate large spurious gradients, and an enormous dynamic range requirement, so it will still be very important to isolate the gradiometer from rotational acceleration. Alternately, one can measure the diagonal terms only, which are not affected by the rotational acceleration; but then one must be careful to avoid contamination by the cross terms, due, for instance, to misalignment of the accelerometer pair.

Another source of error lies in the vertical 3000 E background due to the overall Earth mass. Any slight misalignment of the spacecraft reference frame will project this on the other axes, e.g. 1/2 arc sec will lead to 10^{-2} E. This is not critical in itself, but any fluctuation in alignment at the arc second level could cause serious problems.

3.0 NUMERICAL SIMULATIONS

The numerical simulations being done at SAO use a modified version of the SKYHOOK program, which models the TSS as set of discrete masses and connecting (massless) tether segments. As described in the Final Report to the previous contract, NAG5-325, we have added facility for superimposing spatial fluctuations on the standard atmospheric density routine and outputting the resultant accelerations of the subsatellite, together with ambient densities at each mass, for later analysis. The acceleration components found to be most elucidating are those tangent to the tether at its attachment to the subsatellite and orthogonal. Expressed this way, the effects of tether longitudinal vibrations are separated from the direct effects of atmospheric drag variations. Restrictions are that the subsatellite is considered a point mass (attitude dynamics and aerodynamic effects are not included) and that computational effort limits the number of masses to about 10 for routine use, hence limiting the frequency

response of the system. All cases considered have been limited to a tether deployed in the orbital plane, though this restriction is not inherent in the program.

3.1 Software Modifications

3.1.1 Graphic Capability Enhancement -

One simple, yet important, enhancement of SAO capabilities was the adaptation of graphics tools allowing informative and compact display of the acceleration and spectral outputs. Compare the figures in this report with the hand drawn Figure 7-1 or the printer plots in Appendix D of the NAG5-325 Final Report.

3.1.2 Modification Of Underlying (Mean) Atmospheric Density Routine -

We resolved a subtle problem in the standard SKYHOOK atmospheric density routine which had been causing an occasional sharp jump in the orthogonal acceleration component. The difficulty arose from an interaction of two factors: First, to eliminate residual deployment effects we have been forced to make two SKYHOOK runs for each case considered, a "reference" run with no atmospheric perturbation and a run with the perturbation we wish to study. The resulting accelerations are differenced before plotting, computing spectra or other analysis. Second, the atmosphere routine used simple linear interpolation in a table, resulting in a $\rho(h)$ curve with only piecewise continuous derivative.

Because the two runs are different, the subsatellite will be at slightly different altitudes in each and thus subject to slightly different drag. If both subsatellites are in the same tabular interval, this difference will be constant or vary only very slowly, causing minimal effect. But when one sub-

satellite crosses a tabular altitude, and thus is subject to a different density as function of altitude, this difference in drag takes a sharp jump.

To remedy this problem, we created a smoother atmospheric density routine. We first attempted to simply interpolate $\log(\rho)$, but ended up fitting a moderate order polynomial to the $\log(\rho)$ data (with independant variable $\sqrt{\text{altitude-100km}}$) at each tabulated temperature and interpolating in temperature. This produced the desired smoothness with no noticeable deterioration in execution time. Our scheme of differencing the two runs may still have some effect at very low frequencies, as the relative altitudes of the subsatellites change gradually over the run.

Tracking down this effect of altitude on drag did point up one interesting mechanism:

> Any variation in the subsatellites altitude due to tangent accelerations produced by the tether (approximately vertical) will cause a variation in the ambient atmospheric density, hence the drag experienced, hence the orthogonal (approximately horizontal) acceleration.

3.1.3 Multiple Smooth Perturbations -

The version of SKYHOOK created during the previous contract had allowed only a single density perturbation, with a sharp cutoff between the enhanced (or diminished) region and unperturbed density; the region is elliptical in cross section and extends indefinitely to either side of the orbital plane. Apart from the obvious restriction to a single perturbed region, the sharp boundary results in very long integration time due to the peculiarities of the Gear integrator used to solve the differential equations of motion.

We have extended the allowed perturbations to include up to two hundred (possibly overlapping) regions each with a smooth cutoff to enhance computational efficiency. The parameters of each region are: a vertical radius, r_v; a horizontal radius, r_h; altitude of center, h_c; a distance "along orbit" from the start of the simulation, a_c; and an enhancement factor, e. Again, since we are concerned with deployment in or near the orbital plane, the density perturbations extend indefinitely perpendicular to the plane. First, we define a scaled radius

$$r = \sqrt{((h-h_c)/r_v)^2 + ((a-a_c)/r_h)^2}$$

where h is the altitude and a the "along orbit" distance. Then the density perturbation for a single region, relative to the "base" unperturbed density, is

$$\rho/\rho_{base} = 1 + e/(1+r^2)^2.$$

The region so defined has the same total mass (in a two dimensional sense) as the previous sharply bounded region with the same vertical and horizontal radii and enhancement factor. When there is more than one perturbed region, the right hand side of this equation is computed for each perturbation and they are all multiplied together to form the total perturbation.

3.2 Simulations Of Single Perturbations

We have analyzed four cases: smooth and sharp bounded regions; impinging on the subsatellite at 120 km and on the tether at 170 km altitude. All regions were circular with 20 km (effective) radius, and 20% enhancement.

A typical plot of the residual tangent and orthogonal accelerations experienced after encounter with the perturbation is given in Figure 3-1; the other cases were similar. Note the smoother nature, and much smaller magnitude, of the orthogonal acceleration.

The spectra of the accelerations produced in the various cases are also surprisingly similar. Figure 3-2 shows those for two cases: a smooth perturbation impacting directly on the subsatellite, and a sharply bounded perturbation impacting halfway up the tether. The sharp peaks corresponding to the spring-mass mode and the expected eight longitudinal vibration modes are clearly visible in the tangent acceleration. These unperturbed modes are mimicked by the orthogonal acceleration, with the addition of a mode at very low frequency, possibly due to latitudinal vibration modes. The spectra are largely similar, though the peaks in the case with tether impact are smaller in magnitude; note that the background levels are the same in both cases. To compare in more detail we tabulated the frequencies and magnitudes of the spectral peaks from a printout. The frequencies are all very close, to within ±0.001 Hz. The magnitudes are plotted in Figure 3-3. The disturbances with smooth and sharp cutoffs, at subsatellite altitude, are very similar in both magnitude and relative strengths of the peaks. The disturbance at mid-tether altitude also excites the modes in roughly the same ratios, although with substantially less magnitude.

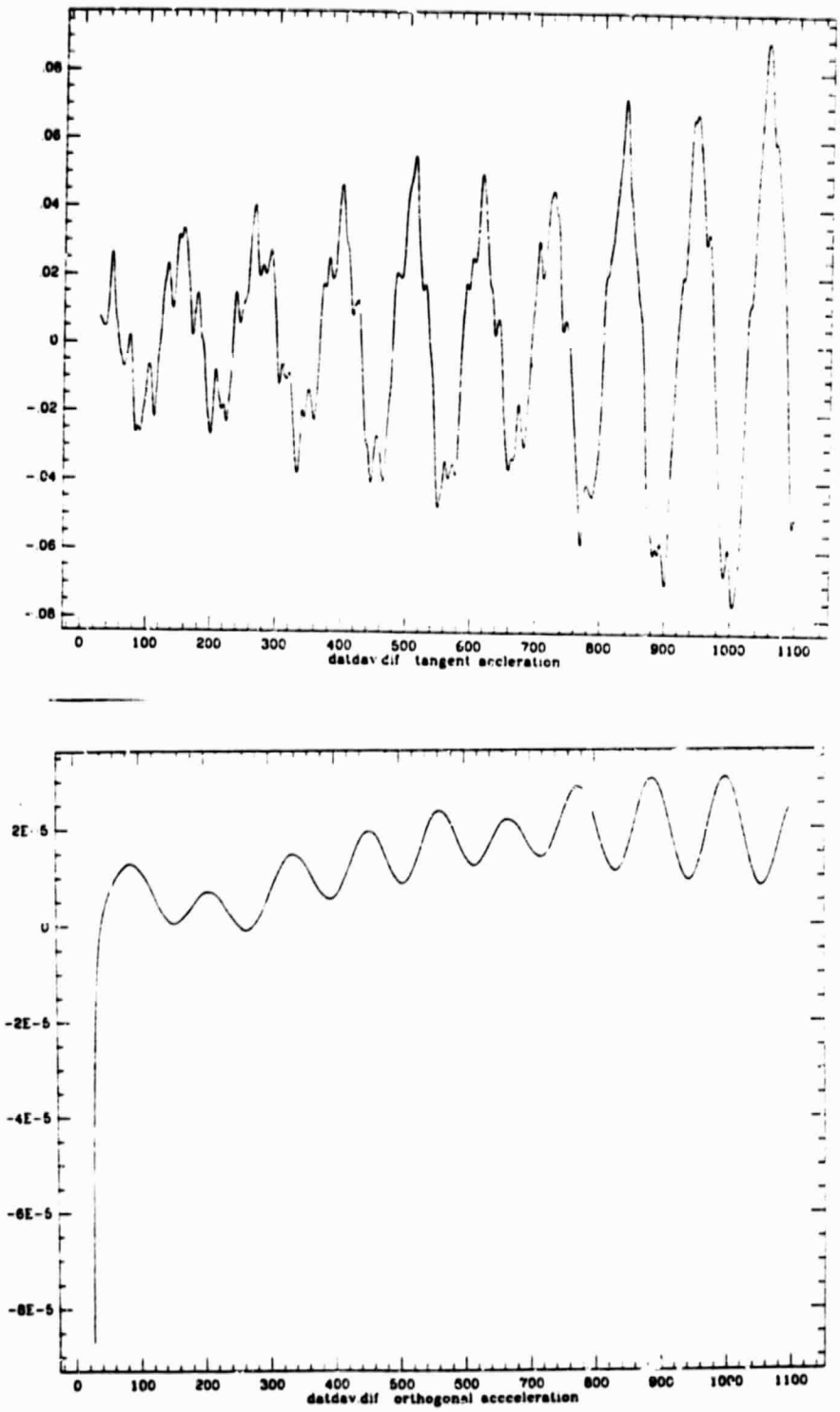

Fig. 3-1. Accelerations, in gals, produced by a single atmospheric density enhancement impacting the subsatellite. Smoothly cutoff region, 20 km radius, 20% enhancement. Acceleration as a function of time is plotted, the component tangent to the tether on top and orthogonal on bottom. Impact with the enhanced region occurred before the data plotted, although some of the final direct effect is visible in the orthogonal component.

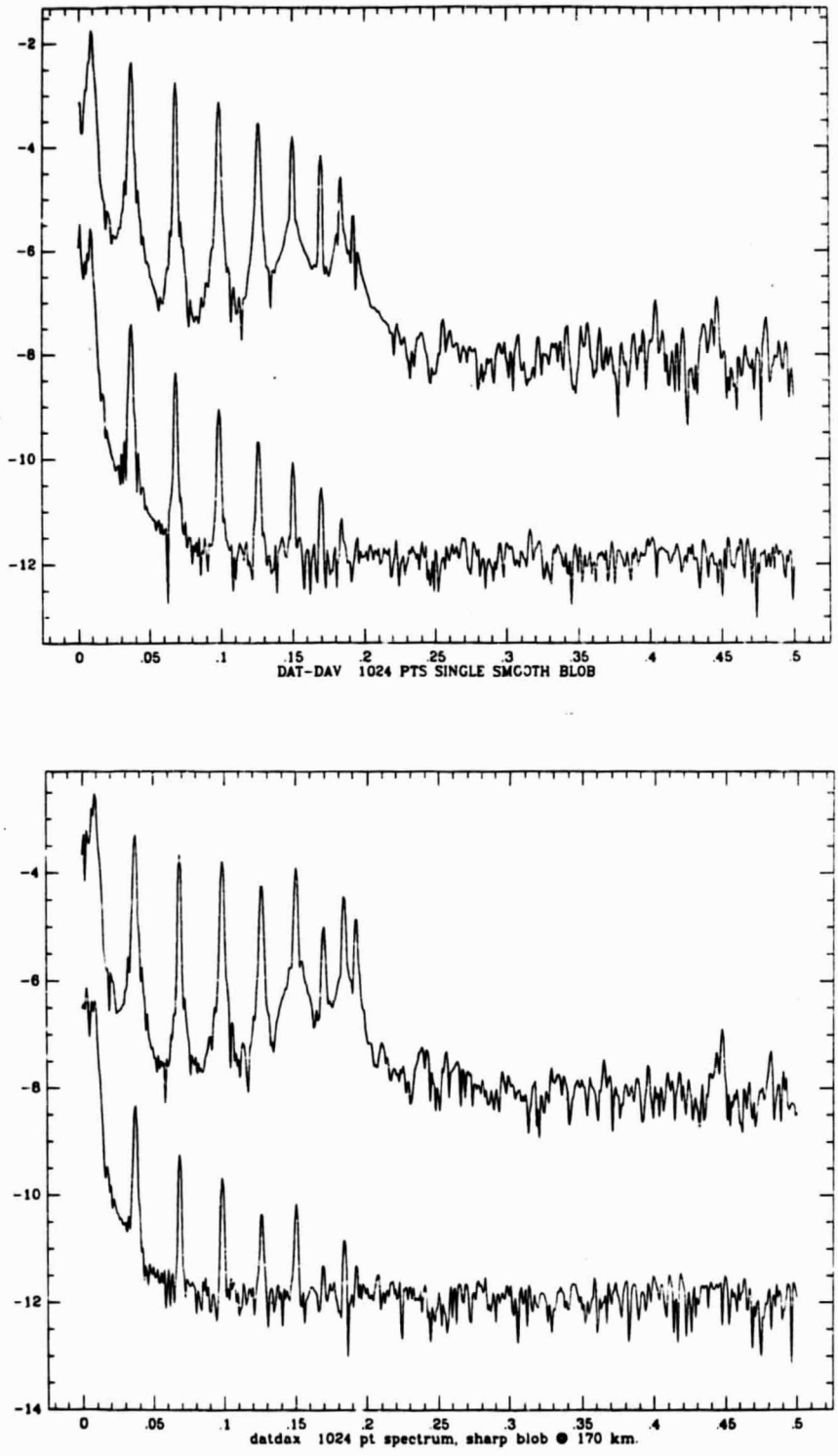

Fig. 3-2. Logarithm of the acceleration spectral magnitude plotted as a function of frequency (Hz). In each plot, the top spectrum is for the tangent component, the bottom for the orthogonal. The top plot is for the case illustrated in Figure 3-1, a single smoothly falling off enhancement impacting directly on the subsatellite. The bottom plot is for an equivalent region impacting on the tether at its center, sharply cut-off to avoid any direct impact on the subsatellite.

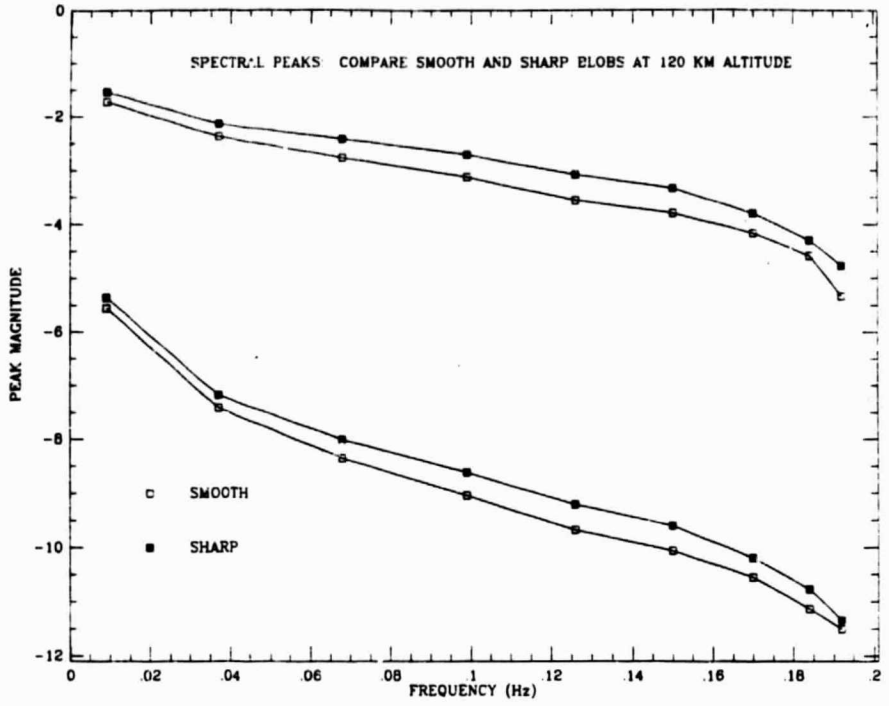

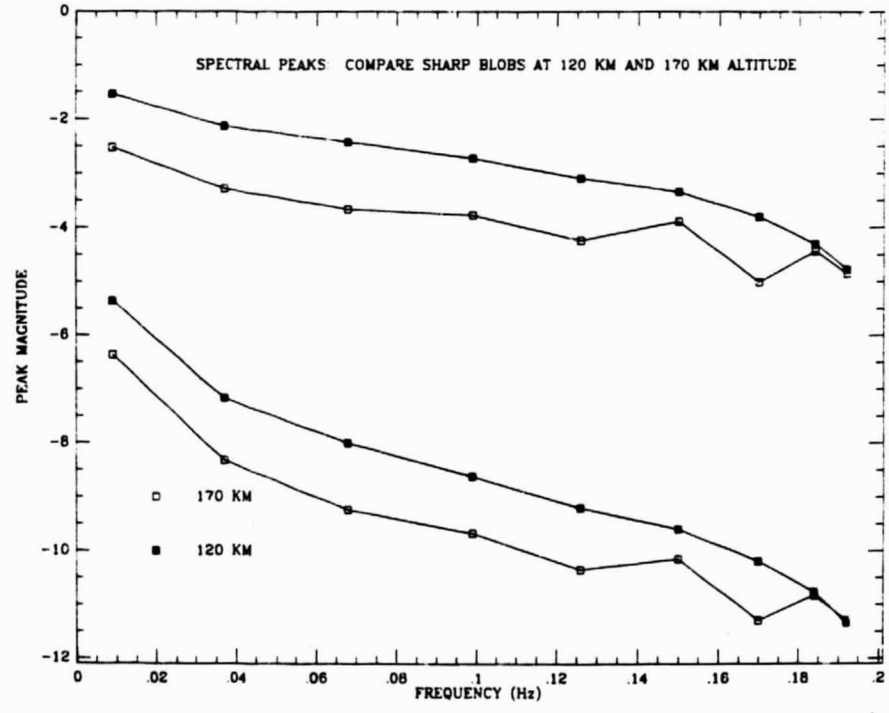

Fig. 3-3. Comparison of the magnitudes of spectral peaks. The peak magnitudes are on logarithmic scales. The top graph compares equivalent regions with sharp and smooth cutoffs, both impacting directly on the subsatellite. The bottom compares identical enhancements impacting on the subsatellite at 120 km altitude and on the tether only at 170 km altitude. In each graph, the top pair of lines is for the tangent component, the bottom for the orthogonal component.

3.3 Modelling A Random Atmosphere

Simulations of encounters with individual "bumps" in the atmospheric density serve to elucidate the impulse response of the TSS. However, it would also be instructive to simulate the TSS passing through a realistic randomly varying atmosphere.

From Gross, Reber and Huang (1984) and Gross and Huang (1985), we know that the power spectral density of variations at 250 km is roughly a power law with exponent -3 at low spatial frequencies and -3 to -4 at higher frequencies. This appears to be the best information available, no similar data existing at the lower altitudes of primary interest to us. The best that can be done, in the absence of some physical theory, is to simply assume the same per-cent variation relative to mean ambient density in the regions of interest.

Creating a random atmosphere by superposing a set of the perturbed regions discussed above was attractive for several reasons:

- By analogy to individule "turbules" in a turbulent medium.
- The individual elements can be implemented and studied before combining them. The superposition is then a relatively simple programming task.
- The Gear integrator used in SKYHOOK demands smooth data for efficient operation. Interpolating on a grid, for instance, would cause much step size and integration order adjustment crossing each mesh line.
- The amount of data needed to represent the atmosphere at a one second time resolution in the horizontal direction and an equivalent distance (say 8 km) vertically is large: roughly 50,000 points for a one hour run.
- Because the Gear integrator, in adjusting step size, may look at intermediate time values after taking one large time step, the density must be effectively created <u>in toto</u> rather than step by step as the simulation proceeds. Having the density at the same place and time change in value depending upon the series of time steps used would be likely to wreak havoc with the integrator's performance.

We have started an investigation of how to create a set of perturbed regions for

use by the current version of SKYHOOK which will have a given spectrum (as seen by the subsatellite traversing the atmosphere). This method appears, in light of these efforts, not to be capable of producing the desired atmosphere model (an individual realization of the random atmosphere).

Two methods appear to show promise, though time was not available to pursue them: First, as an ad hoc approximation assume that the masses in SKYHOOK are at constant altitude. For each mass, create a time series with the desired resolution, interpolate this with a high order spline, and use these separate series. This would still require a substantial amount of data, but would be less strongly interconnected and require no interpolation in the vertical direction. Although acceptable, perhaps, for SKYHOOK with it's limited number of masses, this method could not be extended to simulations requiring greater vertical resolution. Second, the "turning lines method" (see Bras and Rodríguez-Iturbe, 1985) allows reconstruction of a two or three dimensional random field from distributions along a set of lines through a common center; the number of lines suggested is small, 4 to 16. This method is for producing a distribution on a grid, but may be adaptable to our need for densities at unpredictable points.

In the absence of a good theory, we have created a set of 200 regions with random centers (altitudes 120 to 220 km, random distance along track), random radii (up to 30 km vertical, 50 km horizontal) and random enhancement factors (in the range -0.5 to +0.5); all distributions being uniform. The induced accelerations are shown in Figure 3-4, and the spectra in Figure 3-5. The tangent acceleration is roughly similar to that produced by single regions, and in the spectrum we see the same peaks as before although more weakly (note the higher baseline) The same modes are being excited, but with more "noise" generated by the random forcing function. The orthogonal acceleration, however,

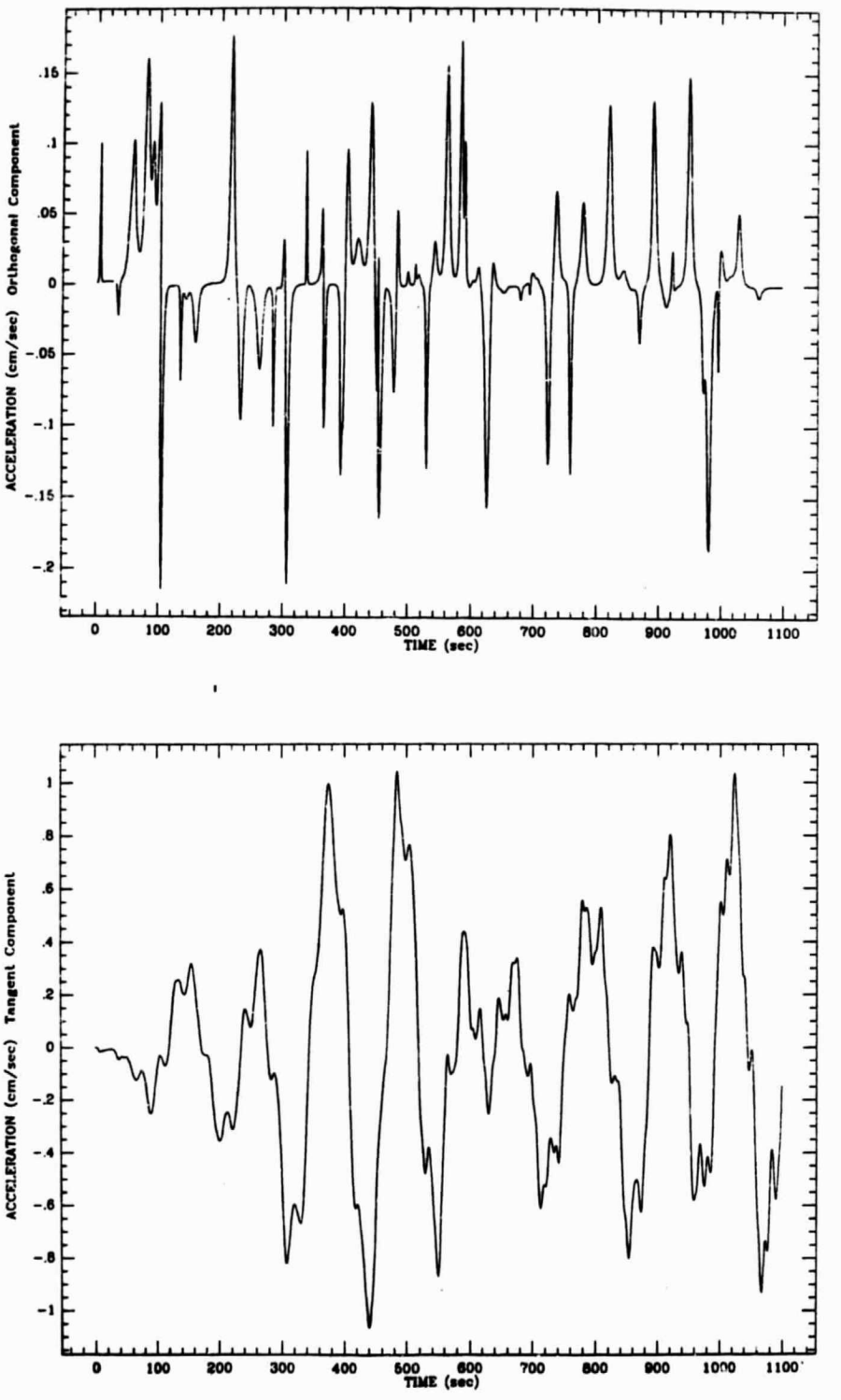

Fig. 3-4. Accelerations produced by a model atmosphere with 200 randomly scattered enhancement regions. The orthogonal component (top graph) appears to be responding directly to the ambient atmospheric perturbation, while the tangent component (bottom graph) is more similar to the results from a single region model (Fig. 3-1).

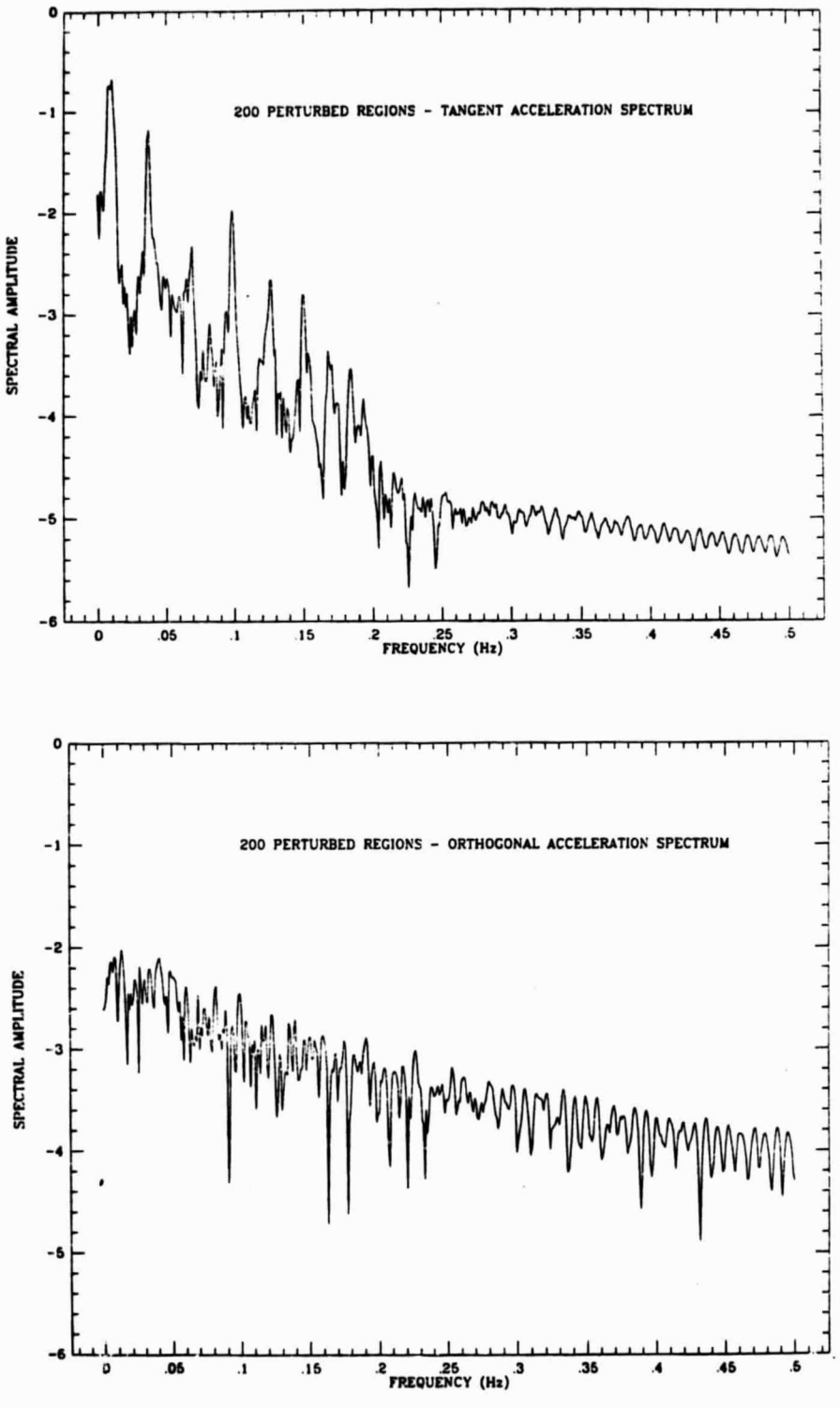

Fig. 3-5. Spectra of the time series in Figure 4. Note that the tangent component spectrum shows distinct peaks corresponding to excited vibration modes, while the orthogonal component spectrum is largely featureless.

is totally dominated by the direct effect of the drag variations, and its spectrum is featureless. For reference, the ambient density at the subsatellite is shown in Figure 6, along with its spectrum. These are similar in character to the orthogonal acceleration, as expected if we are seeing largely direct drag effects in the latter.

4.0 ANALYTIC INVESTIGATIONS

SAO has performed several analytic investigations of tether and TSS system dynamics. These fall in two categories: those aimed at overall understanding of tether dynamics and it's implications for dynamic noise, and those specifically aimed at developing noise abatement methods. We treat the latter first.

4.1 Simple Model For Eliminating Rotational Perturbations

As pointed out in Section 2.1, rotational perturbations of the instrument platform are much more insidious than simple translational accelerations. The SKYHOOK simulations described in Section 3 do not include subsatellite rotation, but it is easy to see that intersection with a density enhancement must cause the subsatellite to rotate: the center of force will be near to the center of the subsatellite, not through the attachment point to the tether, and hence any differential acceleration of the subsatellite and tether will cause a torque.

To alleviate this torque, we adopt the idea of a ballast mass: a second mass attached by a short piece of tether (or rigid rod) to the instrumented subsatellite and with an area/mass ratio chosen so that drag variations will not excite rapid oscillations. We assume that this suspended subsystem is small enough that all points experience the same atmospheric density at any one time,

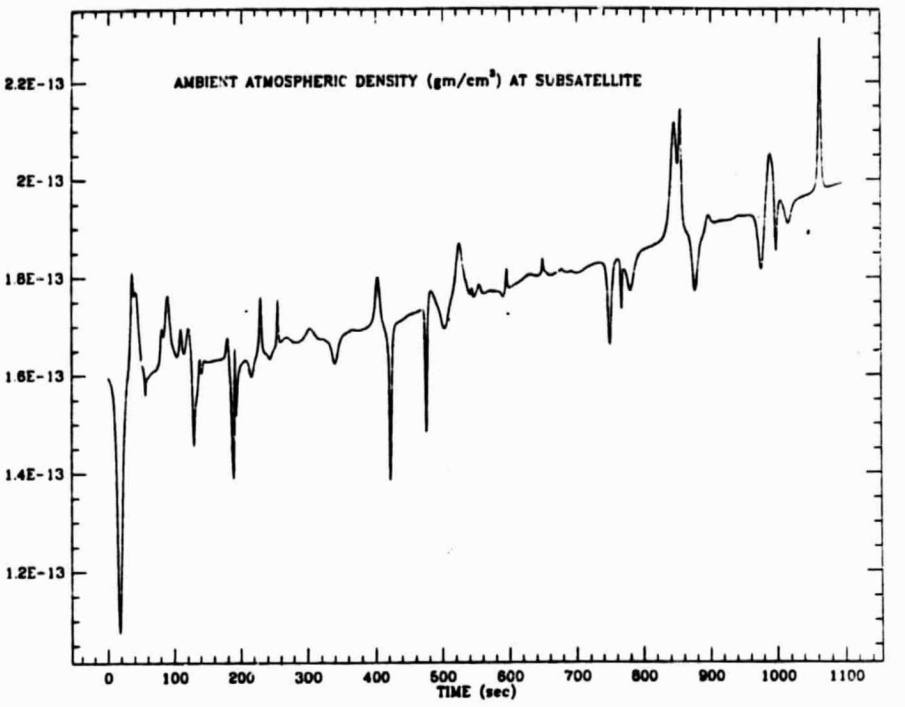

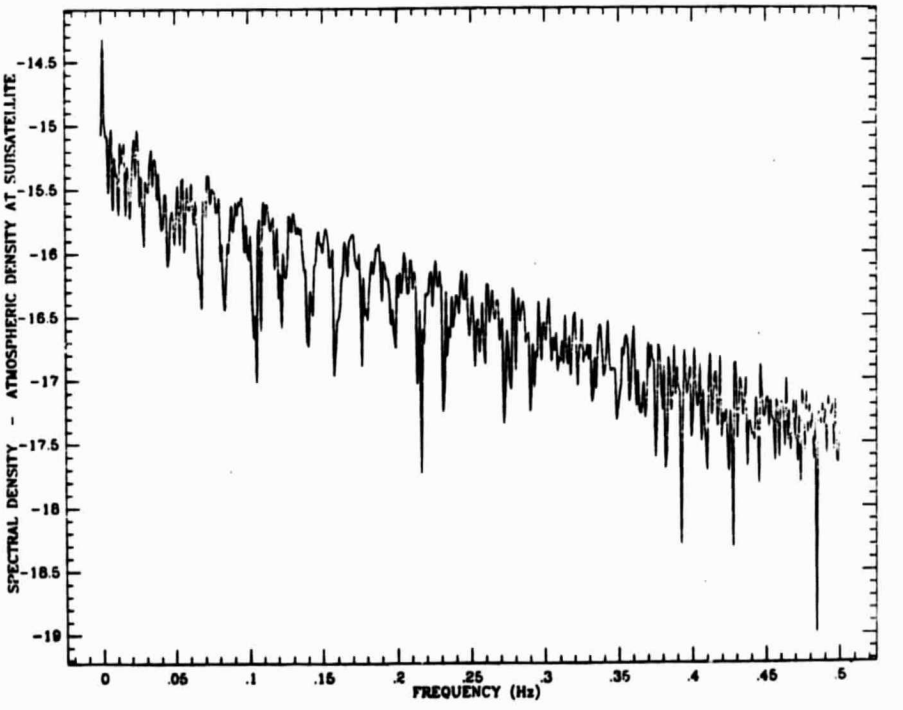

Fig. 3-6. The ambient atmospheric density experienced by the subsatellite in the simulation of Figures 3-4 and 3-5, and its spectrum. Note the similarity to the orthogonal component's graphs in Figures 3-4 and 3-5.

and that the gravity gradient strength (which we shall simply call "g") is uniform.

A full analysis of such a system, some attempts at which are given in the next section, promises to be exceedingly complex, probably being incapable of analytic solution. Here, we present a very simplified model problem which, however, demonstrates the feasibility of the ballast mass idea and illustrates the basic form which a complete engineering analysis would probably follow. The ballast mass concept, and our simple model, are illustrated in Figure 4-1. We model the system as a pair of coupled pendulums suspended from an "infinite mass" Shuttle in the orbital plane, and assume small deviations so that the system becomes linear. We take as the reference configuration simple hanging equilibrium without the complication of the equilibrium displacement due to the mean drag, which should be adequate for the nearly vertical configurations expected. The tether segments are assumed massless and inextensible, and the masses are point masses; the rotation will be apparent in the motion of the angle of the segment joining the two masses. The equilibrium tensions in the two segments, which we may assume to be constant, are

$$T_1 = g(m_1 + m_2)$$
$$T_2 = g\, m_2 \qquad (4.1.1)$$

The system state is fully described by the two angles θ_1 and θ_2. We shall explicitly balance forces in the x (horizontal) direction, and express the result in θ_1 and θ_2. The homogeneous part of the equations is also easily derived via a Lagrangian, leading to the same result. We have:

$$m_1\ddot{x}_1 = -T_1 \sin(\theta_1) + T_2 \sin(\theta_2) + d_1$$
$$m_1\ddot{x}_1 = -T_2 \sin(\theta_2) + d_2 \qquad (4.1.2)$$

To evaluate the left hand sides, use

$$x_1 = L \sin(\theta_1) = L\, \theta_1 \qquad (4.1.3)$$

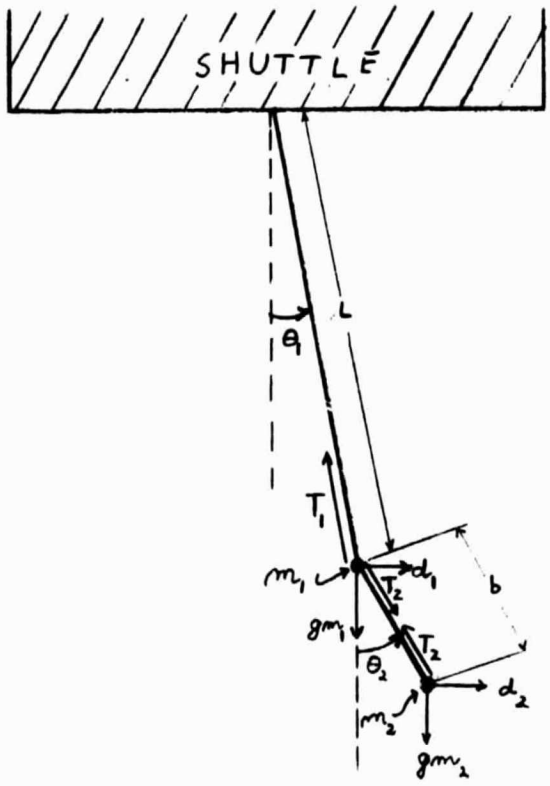

Fig. 4-1. Simplified model of the ballast mass concept for alleviating rotational perturbations due to atmospheric density variations. The system is modelled as two coupled pendulums, with inextensible massless tether segments and point masses.

$$x_2 = x_1 + b\sin(\theta_2) = L\theta_1 + b\,\theta_2$$

and similarly expand the sin() functions on the right hand sides. Use the dimensionless parameters

$$\begin{aligned} \epsilon &= b/L \\ \alpha &= d_1/d_2 = A_1/A_2 \\ \beta &= m_2/m_1 \end{aligned} \tag{4.1.4}$$

where A_1 and A_2 are the cross sectional areas of the two masses; ϵ will be a small parameter, while α and β may be manipulated to achieve desired behavior and are of order unity. Also write $d = d_2$ and $m = m_1$, and after some manipulation obtain:

$$L\begin{bmatrix} 1 & 0 \\ 1 & \epsilon \end{bmatrix}\begin{bmatrix} \ddot{\theta}_1 \\ \ddot{\theta}_2 \end{bmatrix} + g\begin{bmatrix} 1+\beta & -\beta \\ 0 & 1 \end{bmatrix}\begin{bmatrix} \theta_1 \\ \theta_2 \end{bmatrix} = \begin{bmatrix} \alpha \\ 1/\beta \end{bmatrix}\frac{d(t)}{m} \tag{4.1.5}$$

where we explicitly show the dependence of drag on time, d(t). In more concise matrix notation,

$$\mathbf{A}\ddot{\boldsymbol{\theta}} + \mathbf{B}\boldsymbol{\theta} = \mathbf{a}\,d(t) \tag{4.1.6}$$

To solve this system of equations we shall assume that it is initially at rest and apply the Laplace transform

$$\mathcal{L}[f(t)] \equiv F(r) \equiv \int_0^\infty e^{-rt} f(t)\,dt \tag{4.1.7}$$

Using the properties

$$\begin{aligned} \mathcal{L}[f'(t)] &= -f(0) + rF(r) \\ \mathcal{L}[f''(t)] &= -f'(0) - rf(0) + r^2F(r) \end{aligned} \tag{4.1.8}$$

along with the initial conditions, and letting

$$\begin{aligned} D(r) &= \mathcal{L}[d(t)] \\ \boldsymbol{\Theta}(r) &\equiv [\Theta_1, \Theta_2]^T = \mathcal{L}[\boldsymbol{\theta}(t)] \end{aligned} \tag{4.1.9}$$

we find

$$r^2\mathbf{A}\boldsymbol{\Theta} + \mathbf{B}\boldsymbol{\Theta} = \mathbf{a}D(r) \tag{4.1.10}$$

This is an <u>algebraic</u> equation for $\Theta(r)$, and can be solved to give

$$\begin{bmatrix} \Theta_1 \\ \Theta_2 \end{bmatrix} = \frac{1}{\Delta} \begin{bmatrix} Lr^2\epsilon+g & g\beta \\ -Lr^2 & Lr^2+g(1+\beta) \end{bmatrix} \begin{bmatrix} \alpha \\ 1/\beta \end{bmatrix} \frac{D(r)}{m} \tag{4.1.11}$$

where

$$\Delta \equiv (Lr^2 + g(1+\beta))\ (Lr^2\epsilon + g) + g\beta Lr^2 \tag{4.1.12}$$

We are specifically interested in Θ_2:

$$\Theta_2(r) = \frac{(Lr^2 + g(1+\beta))/\beta - \alpha Lr^2}{\Delta} \frac{D(r)}{m} \tag{4.1.13}$$

To progress further, we assume a simple impulse, $d(t) = d_0\,\delta(t-T)$. Then $D(r) = d_0 e^{-Tr}$. For the moment, let $d_0 = m = 1$; if needed, linearity of the Laplace transform would let us factor them in after the answer is obtained. Also, we can let $T = 0$, since the factor e^{-Tr} in the Laplace transform simply shifts the time-domain function by T: $\mathcal{L}^{-1}[e^{-Tr}\,F(r)] = f(t-T)$. Thus, we may take $D(r)/m = 1$ in (4.1.13).

We now need the inverse Laplace transform of the (known) $\Theta_2(r)$. From here on, <u>we shall assume $\epsilon \ll 1$, that is $b \ll L$</u>. Then we factor the denominator to lowest order in ϵ:

$$\Delta = \epsilon L^2\ (r^2 + e^2)\,(r^2 + f^2) \tag{4.1.14}$$

where

$$e^2 = \frac{g(1+\beta)}{L\epsilon} = \frac{g(1+\beta)}{b}$$
$$f^2 = \frac{g}{L} \tag{4.1.15}$$

As we shall see below, f represents a slow mode of overall oscillation, while e gives a fast mode of subsatellite oscillation. Noting that

$$\frac{1}{(r^2+e^2)\,(r^2+f^2)} = \frac{1}{f^2-e^2}\left[\frac{1}{r^2+e^2} - \frac{1}{r^2+f^2}\right] \tag{4.1.16}$$

and that $f^2-e^2 = -e^2$ to lowest order in ϵ, and letting

$$h^2 = \frac{g(1+\beta)}{L(1-\alpha\beta)} \tag{4.1.17}$$

we find after considerable algebra:

$$\Theta_2(r) = -\left[\frac{1-\alpha\beta}{g\beta(1+\beta)}\right]\left[\frac{h^2-e^2}{r^2+e^2} - \frac{h^2-f^2}{r^2+f^2}\right] \tag{4.1.18}$$

Putting the factor $d\theta_0 L/m$ back into the answer, and using $\mathcal{L}^{-1}[1/(r^2+a^2)] = (1/a)\sin(at)$, we obtain

$$\theta_2(t) = -\left[\frac{d_\theta}{fm}\right]\left[\frac{1-\alpha\beta}{\beta(1+\beta)}\right]\left\{\left(\frac{h^2-e^2}{e}\right)\sin(et)\left(\frac{h^2-f^2}{f}\right)\sin(ft)\right\} \qquad (4.1.19)$$

We have two parameters, α and β, at our disposal and we use them to eliminate the fast mode corresponding to $\sin(et)$ by setting $h^2-e^2 = 0$, which leads to $\alpha\beta = 1-\epsilon$, or

$$\frac{m_2}{A_2} = (1-\epsilon)\frac{m_1}{A_1} \qquad (4.1.20)$$

to first order in ϵ.

This answer is in some sense obvious, to zero'th order in ϵ: for the masses to accelerate equally, neglecting the suspending tether, their mass/area ratios must be equal. What we have done here is to derive a first order approximation and, more importantly, illustrated techniques that might be used in a more complicated and realistic calculation. The fact that we have been able to eliminate the fast mode in this first order calculation, as well as the zero'th order one, also is promising for success in eliminating fast rotational modes in more complete models.

Before leaving this very simple model, we should consider one last question: What is L? Most simply, if the assumption of a massless, inextensible tether were precise, L would simply be the distance from the subsatellite to the shuttle. The real tether, however, will have an influence and an L useful for back-of-the-envelope calculations might be taken as, say, the length of tether whose mass equals the subsatellite (not substantially different in the case of a 100 km tether with density 8 kg/km and a 500 kg subsatellite), or the wavelength of transverse waves having the same period as the subsatellite pendular oscillation (which is much smaller: for a subsatellite with 0.2 Hz oscillations and a tether with spectrum 0.001n Hz, this gives mode n=200, or wavelength about 1/2

km). Providing a confident answer to this question will depend on experience from sample calculations including a continuum tether; the beginnings of such calculations are discussed in the next section.

4.2 Extensions To The Simple Model

In the above section we have demonstrated the feasibility of using a ballast mass to help eliminate rotational perturbations of the subsatellite instrument platform by atmospheric density variations. A great deal remains to be done before such abatement methods can be considered fully designed.

Still within the context of non-continuum tethers, one could add to the model such factors as tether elasticity and damping, rotational dynamics of the subsatellite and ballast, and more complicated arrays of ballast masses (e.g., one below and one above the instrument platform) and specially designed connecting elements (such as highly damped cables). Such complications are likely to soon reach the limits of analytic solubility and require numerical solution and various numerical parameter optimization methods.

Adding the continuum tether adds another whole level of complexity, requiring solutions to mixed partial and ordinary differential equations, but must be done before the problem can be considered fully explored. We have achieved a partial solution of a simple case: one point mass on the end of a tether with no damping and no body forces (drag, gravity), hanging from an infinite mass shuttle. The suspended mass experiences a variable drag d(t).

We shall not give our calculations in detail. The oscillations in the three orthogonal directions are decoupled (for small displacements), and only the horizontal, along-orbit direction is effected by d(t). The equations for

this component are:

$$\mu v_{tt} = (T_o \ell / L)\, v_{ss} \qquad 0 \le s \le \ell$$

$$v(0,t) = 0$$

$$v(\ell,t) = \eta(t)$$

$$m\,\ddot{\eta}(t) = -(T_o \ell / L)\, v_s(\ell,t) + d(t)$$

where ℓ is the tether's natural length, L its stretched length in equilibrium, T_o the equilibrium tension, $\eta(t)$ the displacement of the end mass, and the rest of the notation follows previous discussion. Laplace transforming this system with respect to time generates an ordinary differential equation with τ as a parameter:

$$\tau^2 V(s,\tau) = c^2\, V_{ss}(s,\tau) \qquad 0 \le s \le \ell$$

$$V(0,\tau) = 0$$

$$V(\ell,\tau) = E(\tau)$$

$$\tau^2\, E(\tau) = -b^2\, V_s(\ell,\tau) + D(\tau)$$

where V and E are Laplace transforms of v and η, D is the transform of d(t)/m, and b and c are constants. This system is readily soluble to give

$$V(s,\tau) = \left[\frac{D(\tau)/\tau^2}{\sinh(\tau\ell/c) + (b^2/\tau c)\cosh(\tau\ell/c)} \right] \sinh(\tau s/c)$$

$$E(\tau) = \frac{D(\tau)}{\tau^2} \frac{\sinh(\tau\ell/c)}{\sinh(\tau\ell/c) + (b^2/\tau c)\cosh(\tau\ell/c)}$$

We are primarily interested in the motion of the mass and thus in the inverse transform of $E(\tau)$. Unfortunately, even for simple forms of $D(\tau)$ this does not seem to be tabulated nor to be modifiable to a recognizable form. Further investigation may provide an analytic solution, but fully realistic calculations with systems of suspended, finite extent masses will likely require numerical approaches. A modal (separation of variables) analysis should also be made to attempt to find the response to a drag impulse.

4.3 Cooperation With Prof. Silvio Bergamaschi

In December 1984 Prof. Silvio Bergamaschi of the Institute of Applied Mechanics in Padova, Italy visited SAO. Though NAG5-458 provided no direct funds for his visit, we did spend several days discussing tether dynamics, particularly dynamic noise, with Prof. Bergamaschi. Prof. Bergamaschi is developing a model of the TSS including a full continuum tether with end masses, and gravity gradient force on the tether itself. Modal analysis is being applied to this model. We assisted him with some numerical mode calculations, and discussed some non-intuitive physical implications of the results. We hope to continue the cooperation in developing this model, which will provide both a valuable check on SKYHOOK numerical computations, and results not obtainable with SKYHOOK. In the future we hope to cooperate with Prof. Bergamaschi on measurement and analysis of the TSS dynamic environment during the TSS Demonstration Flights.

4.4 Effects Of Tether Internal Damping

Our simulations and analytical calculations have ignored the effect of energy dissipation within the tether. The simplest form of such dissipation would be internal viscous damping. This has been partially because of the added complications this would introduce and partially because of uncertain knowledge of tether properties. We have, however, made some simple theoretical calculations which we present here and which indicate that tether viscous damping may be quantitatively significant though probably not qualitatively crucial to understanding of dynamic noise. (Some of the work in this section has been performed in conjunction with NASA Contract NAS8-36160, and a portion of this sec-

tion has been excerpted from Quarterly Reports 2 and 3 of that contract.)

We begin at the very beginning, and derive the equations governing a tether with internal viscous damping. Though certainly not new, this material does not seem to be readily available (typical sources give equations for cables subject to external damping, such as an ambient fluid). First we consider a tether segment, for the moment considered massless; later we shall derive the partial differential equation for a continuum tether. We wish to derive the dependance of the damping constant for a piece of tether material on the length of the piece, under some very general assumptions. Specifically, we assume that the material is viscous but not plastic. That is, there will be resistance to motion, but no permanent change in the equilibrium state. We assume a simple Hooke's law form for the elastic portion of the stress, and the viscous damping will add a term proportional to velocity.

Consider a simple physical system: a length of tether fastened to a wall at one end and a mass M at the other. Neglect the tether mass. Let x be the extension of the segment past natural length. Then the equation of motion is

$$M\ddot{x} = -Kx - B\dot{x} \qquad (4.4.1)$$

where K is the Hooke's law spring constant and B is some damping constant. Now suppose we cut the tether in its center and place a small mass m between the pieces; denote the extension of the segment between the wall and mass m by y. Then the equations of motion are twofold:

$$\begin{cases} M\ddot{x} = -k(x-y) - b(\dot{x}-\dot{y}) \\ m\ddot{y} = -ky - b\dot{y} \\ \qquad\quad +k(x-y) + b(\dot{x}-\dot{y}) \end{cases} \tag{4.4.2}$$

If we let $\xi = (x-y)$, a bit of manipulation arrives at the equation

$$M\ddot{x} = -\tfrac{1}{2}kx - \tfrac{1}{2}b\dot{x} - \tfrac{1}{2}m(\ddot{x} - \ddot{\xi}) \tag{4.4.3}$$

Let $m \to 0$ and compare the result to equation (1). If the accelerations in the third term of (3) remain finite, which we shall simply assume since this is not meant to be a rigorous proof, agreement between these two results for the motion of mass M requires that $k = 2K$, $b = 2B$. Generalizing the argument, we have that

$$k \propto \frac{1}{\ell} \qquad b \propto \frac{1}{\ell} \tag{4.4.4}$$

where ℓ is the (natural) length of the tether segment. For the spring constant k, the proportionality constant is simply EA, Young's modulus times the cross sectional area. For the damping constant b, we shall follow a remark in Bodley and Park (1983; p. 54) and denote the proportionality constant by C_v. (Note that EA and C_v apply to a tether of given cross section and manufacture. It seems reasonable that the energy dissipation, hence the resistive force, will be proportional also to the cross sectional area of the tether; we may expect that $c_v \equiv C_v/A$ is a material constant analogous to E.)

Now let us derive the partial differential equation for longitudinal motion of a tether with viscous damping, considered as a continuum. We suppose that the tether remains in a straight line, and is sufficiently extended in its equilibrium state (e.g., by loading) so that it does not go slack for small perturbations. Let u(s,t) be the <u>displacement</u> from equilibrium of a mass element which would be at coordinate s in equilibrium; thus the full position will

be $x(s,t) = s + u(s,t)$. The tether has properties AE and C_v as above, and mass per unit length μ.

Apply the lumped mass or ball-and-spring approximation to the continuum tether, with masses separated by $\Delta s = h$. The mass of each particle is then μh, and denote it's displacement from equilibrium by $U_i(t)$. The acceleration of a particular mass will then be given by the sum of the spring forces and damping of the two tether segments on each side; these will each have $k = AE/h$ and $b = C_v/h$.

$$\begin{aligned} \mu h \ddot{U}_i = \quad & + (AE/h)(U_{i+1}-U_i) \quad + (C_v/h)(\dot{U}_{i+1}-\dot{U}_i) \\ & - (AE/h)(U_i-U_{i-1}) \quad - (C_v/h)(\dot{U}_i-\dot{U}_{i-1}) \end{aligned} \tag{4.4.5}$$

leading to

$$\mu \ddot{U}_i = (AE)\left[\frac{U_{i+1} - 2U_i + U_{i-1}}{h^2} \right] + C_v\left[\frac{\dot{U}_{i+1} - 2\dot{U}_i + \dot{U}_{i-1}}{h^2} \right] \tag{4.4.6}$$

$$\doteq (AE) \frac{\partial^2 U_i}{\partial s^2} + C_v \partial^2 \dot{U}_i / \partial s^2$$

In the limit as $h \to 0$, this becomes a damped wave equation:

$$\mu \frac{\partial^2}{\partial t^2} u(s,t) = \left[AE + C_v \frac{\partial}{\partial t} \right] \frac{\partial^2}{\partial s^2} u(s,t) \tag{4.4.7}$$

We are now able to examine the effects of damping. Consider a tether of length L, with fixed ends as a "standard" case. With $a \equiv AE/\mu$ and $b \equiv C_v/\mu$, the PDE becomes $u_{tt} = (a + b\partial/\partial t)\, u_{ss}$. Standard separation of variables with $u(s,t) = S(s)T(t)$ yields modes

$$\begin{aligned} S_n(s) &= \sin(\kappa_n s) \\ T_n(t) &= \exp(\alpha(\kappa_n)\, t) \end{aligned} \tag{4.4.8}$$

where

$$\begin{aligned} \kappa_n &= n\,\pi/L \\ \alpha(\kappa) &= (1/2)\left[-\kappa^2 b \pm \sqrt{(\kappa^2 b)^2 - 4\kappa^2} \right] \end{aligned} \tag{4.4.9}$$

The wavelength of a mode associated with κ is just $W = 2\pi/\kappa$.

Note that for κ, corresponding to the longest wavelength modes, the square root in (4.4.9) is imaginary and the modes will be oscillatory. For non-zero damping, though, the higher modes will be overdamped with no oscillatory behavior. This occurs when the square root becomes real, at

$$W_{CRIT} \equiv \pi\ C_V\ /\ \sqrt{\mu AE}$$
$$n_{CRIT} = 2L/W_{CRIT} \qquad (4.4.10)$$

Note that this critical wavelength for damping depends only on the tether properties and not on the length of tether involved; the total length determines only how many oscillatory modes will actually exist. Of related interest is the maximum achievable frequency of an oscillatory mode. The frequency, that is the imaginary part of $\alpha(\kappa)$, is zero for κ=0, rises to a maximum value, and declines to zero at $\kappa = 2\pi/W_{CRIT}$; above this, the modes are not oscillatory. This maximum value is

$$\omega_{max} = AE/C_V \qquad (4.4.11)$$

To evaluate these quantities we need estimates of the tether properties, particularly the damping C_V. We have two sources of information as to the damping in the tether material, both provided by Martin Marietta Corporation. These sources appear to differ substantially.

First, there is a June 1983 report (Bodley and Park, 1983) which uses a value $C_V = 9.19 \times 10^4$ at one point in its analysis (p. 54); the source of this number is not clear, and it may be a preliminary value. Second, an internal report (Martin Marietta Corporation, 1983) dated September 1983 was kindly provided by A. C. Park of MMC; this report gives a "per cent damping" for an experimental setup consisting of a mass hanging on the end of a length of tether. We have calculated the damping coefficient from the experimental report (but see the caveats below), and converted the earlier number to the same (mks) units. In summary:

- From the experimental data, AE $\approx 10^5$ kg-m/s^2 and $C_v \sim 200$ kg-m/s ("averaging" the experiments described). These imply a critically damped wavelength for tether longitudinal oscillations of about 25 meters (say, between 10 and 100), and a maximum oscillatory frequency of about 300 sec^{-1}.

- The value $C_v = 9.19 \times 10^4$ kg-km/hr given in the "... Orbital Dynamics ..." report, when converted to mks system becomes 2.6×10^4 kg-m/s. This is about 100 times greater than the value calculated from the experimental data above. The critically damped wavelength implied is about 3 km and the maximum oscillation frequency is about 4 sec^{-1}. (The values for AE and μ, converted to mks, are consistent with the experimental AE and assumed 3 mm Kevlar at 1.5 g/cc density.)

Our interpretation of the experimental results, however, is somewhat uncertain since (1) the precise testing and computation procedures used were not clear, and (2) neither the direct experimental results nor a derived material property (C_v) were reported, but a "per cent damping", presumably the damping ratio for the experimental setup consisting of a 4.5 kg mass on the end of an 11 or 21 m "spring."

In summary, we can say that viscous damping (and possibly other forms of energy dissipation such as friction among the strands of the yarn-like tether) can alter the frequencies of longitudinal oscillation modes. The available values for the damping coefficient span a wide range, and the maximum oscillation frequency corresponding to the larger of the two values is close enough to frequencies of interest (1 second period or frequency $1/2\pi$) to be of have substantial impact. A clearer determination of tether damping properties, particularly in a space environment, would be of value.

5.0 MISCELLANEOUS EFFORTS

5.1 Random Vibration Analysis:

The methods we have been using, and which have been discussed so far in this report, are all deterministic in the sense that we consider a given input (the atmospheric density as a function of position), make computations with a computer simulation program or an analytical model, and observe the result (accelerations or rotations). The density may be a simple localized enhancement, or it may be a complicated randomized function, but during the analysis it is fixed; statistical information would need to be garnered from repeated simulations, or (equivalently under stationarity assumptions) from observing isolated sections of a single long simulation.

Random vibration analysis, which takes into account explicitly the random nature of the input, is also likely to be useful. Both the atmospheric density variations and the resulting subsatellite acceleration and rotation are random processes. The system connecting input and output is still deterministic, but rather than simulating the response to an individual realization of the input process to achieve an individual realization of the output, we provide a statistical description of the input process and gain a statistical description of the output process.

This resulting statistical information complements the specificity of individual case studies. With it we can derive information of use in designing instruments, such as the expected time to first excursion to a given response level (which might, for instance damage or saturate an instrument) or failure due to accumulated stress. Also, the perturbations to the instrumental output can then be analyzed to determine their effect on the gravity field after final

data analysis. Finally, such considerations might elucidate the knowledge of the atmospheric fluctuations required, either from further experiment (or re-analysis of old data) or from theoretical arguments (such as gravity wave models).

Performing such analyses of the dynamically complicated TSS is likely to require substantial effort, but the results promise to be of substantial value. An early monograph on the subject, lucid but limited, is Crandall and Mark (1963). More complete and recent works are Lin (1967) and Nigam (1983).

6.0 DIRECTIONS FOR FUTURE RESEARCH

As with any major project, the possible tasks seem to increase as work is done. We make here some suggestions for future workers in the field. SAO hopes to continue dynamic noise studies in connection with the TSS Demonstration Missions either under direct contract or in cooperation with other investigators such as Prof. Bergamaschi.

Improvements in simulation capabilities could proceed along two lines:

First, a simplified, streamlined and enhanced program similar to SKYHOOK is in order. Much of SKYHOOK's broad capabilities are of little importance to dynamic noise analysis and only inhibit investigation of the features of interest as well as making program maintenance a burden. For situations with rapidly varying forcing functions the Gear method may not be the best (other methods such as Runge-Kutta-Fehlberg exist for stiff systems); even if it is, the specific subroutine should be tuned to avoid such frequent step size and order changes. The system of equations in SKYHOOK is in actuality not merely stiff but stiffly oscillatory. There appear to be no general purpose routines or

methods for such systems, but there is some promise of developing a special purpose method for tethered systems. The data structure should be changed to allow use of off-the-shelf band matrix techniques (or special routines written). Subsatellite rotational and aerodynamics should be added, as well as the facility for multiple mass subsatellite systems. Rotational effects, particularly rotational acceleration, are of key importance in gravity gradiometry. Generating equilibrium initial conditions would avoid the current differencing with a reference simulation.

Second, although not a classical form of simulation, the random vibration methods should be attempted. The statistical results obtained would provide a valuable alternate view to the case studies possible with SKYHOOK like programs.

For case study simulations, realistic sample atmospheres should be generated. Superposition of moderate numbers of local enhancements seems to be of limited worth. Methods of generating and using a large grid of (smooth) random densities should be explored, including the ad hoc method suggested in Section 3.3 and the Rotating Lines Method. Also, apart from the question of generating random atmospheres, it would be worthwhile to add a damped wave (or set of such) to the perturbation options. This feature is suggested by observations of Gross and Huang (1984).

The tools for analyzing the results of simulation runs can be simplified and streamlined. On a more fundamental level, use of the Maximum Entropy Method for spectral analysis seems very promising. Both theory and the experience shown in our figures indicate that we should expect a number of sharp peaks on a smoother background. This sort of spectrum is ideally suited to MEM techniques, which effectively use rational function approximations to the spectrum rather than the simple polynomial approximation of Fourier analysis, and are thus bet-

ter able to represent sharp peaks or lines. (Press, et al., 1985.) MEM is likely to be useful also for analyzing actual data from a physical gradiometer.

Design of stabilizing ballast configurations will involve complicated analytical studies, probably eventually requiring numerical work for realistic designs. Detailed study of mixed partial and ordinary differential systems may derive some rules which may be applied to estimate the effects of the continuum tether without requiring the full formality.

7.0 REFERENCES

Bodley, C. S., and Park, A. C., Analysis of Tethered Satellite System Orbital Dynamics for Selected Mission Profiles, Report TSS-83-ACP-065, Martin Marietta Denver Aerospace, June 1983.

Bras, Rafael L. and Rodríguez-Iturbe, Ignacio, 1985. Random Functions and Hydrology, Reading, Massachusetts: Addison-Wesley Publishing Company, §6.6.

Crandall, Stephen H. and Mark, William D., 1963. Random Vibrations in Mechanical Systems, New York: Academic Press.

Gross, S. H., Reber, C. A. and Huang F. T., 1984. "Large-Scale Waves in the Thermosphere observed by the AE-C Satellite," IEEE Trans. Geosci. Remote Sensing, vol. GE-22, pp. 340-352.

Gross, S. H. and Huang F. T., 1985. "Medium Scale Gravity Waves in the Thermosphere Observed by the AE-C Satellite," IEEE Trans. Geosci. Remote Sensing, vol. GE-23, pp. 139-149.

Lin, Y. K., 1967. Probabilistic Theory of Structural Dynamics, New York: McGraw Hill, Inc. (Reprint, 1976 with corrections: Huntington, New York: Robert E. Krieger Publishing Co., Inc.).

Martin Marietta Corporation, 1983. Tether Testing, report dated September 1983.

Nigam, N. C., 1983. Introduction to Random Vibrations, Cambridge, Massachusetts: The MIT Press.

Press, William H., Flannery, Brian P., Teukolsky, Saul, and Vetterling, William T., 1985 (in press). Numerical Recipes: Methods for Numerical Computation, Cambridge (UK): Cambridge University Press, §12.8.